ELSEVIER

Neuroscience Research 34 (1999) 103–113

NEUROSCIENCE RESEARCH

www.elsevier.com/locate/neures

In vivo imaging of spontaneous ultraweak photon emission from a rat's brain correlated with cerebral energy metabolism and oxidative stress

Masaki Kobayashi [a,*], Motohiro Takeda [a], Tomoo Sato [a], Yoshihiko Yamazaki [b], Kenya Kaneko [b], Ken-Ichi Ito [b], Hiroshi Kato [b], Humio Inaba [a,c]

[a] *Yamagata Advanced Technology Research and Development Center, 2-2-1 Matsuei, Yamagata 990-2473, Japan*
[b] *Department of Physiology, Yamagata University School of Medicine, 2-2-2 Iida-nishi, Yamagata 990-9585, Japan*
[c] *Tohoku Institute of Technology, 35-1 Yagiyama-kasumi-cho, Taihaku-ku, Sendai 982-8577, Japan*

Received 17 December 1998; accepted 14 April 1999

Abstract

Living cells spontaneously emit ultraweak light during the process of metabolic reactions associated with the physiological state. The first demonstration of two-dimensional in vivo imaging of ultraweak photon emission from a rat's brain, using a highly sensitive photon counting apparatus, is reported in this paper. It was found that the emission intensity correlates with the electroencephalographic activity that was measured on the cortical surface and this intensity is associated with the cerebral blood flow and hyperoxia. To clarify the mechanism of photon emission, intensity changes from whole brain slices were examined under various conditions. The removal of glucose from the incubation medium suppressed the photon emission, and adding 50 mM potassium ions led to temporal enhancement of emission and subsequent depression. Rotenone (20 μM), an inhibitor of the mitochondrial electron transport chain, increased photon emission, indicating electron leakage from the respiratory chain. These results suggest that the photon emission from the brain slices originates from the energy metabolism of the inner mitochondrial respiratory chain through the production of reactive oxygen. Imaging of ultraweak photon emission from a brain constitutes a novel method, with the potential to extract pathophysiological information associated with neural metabolism and oxidative dysfunction of the neural cells.

Keywords: Biophoton; Chemiluminescence; Cerebral metabolism; Reactive oxygen; Oxidative stress; Imaging

1. Introduction

It is known that living organisms emit ultraweak light spontaneously during metabolic reaction processes without any external excitation or administration of chemiluminescent agents. The process is referred to as 'biophoton emission' (Cilent, 1988; Inaba, 1988; Popp, 1988; Popp et al., 1988; Slawinski, 1988; Van Wijk and Schamhart, 1988; Usa et al. 1994; Devaraj et al., 1997).

The intensity of the emission is estimated to be less than 10^{-16} W/cm^2 on the surface. The biochemical mechanism by which biophotons are emitted is broadly categorized as chemiluminescence. This can be differentiated from the bioluminescence phenomena observed in, for example, fireflies or luminescent bacteria, which have distinctive mechanisms for providing luminescence through an enzymatic reaction (luciferin–luciferase) system that has a high quantum yield.

Electronically excited states of constituents of living cells are generally derived from oxidative metabolism that accompanies the production of reactive oxygen species (ROS; $O_2^{-\bullet}$, H_2O_2, $OH^{\bullet}$, $^1O_2$). In regular energy metabolism, cellular respiration, a reaction in the electron transfer chain of the inner mitochondrial membrane, participates in ROS production, which is facilitated especially under the highly reduced state of an electron transfer chain.

* Corresponding author. Tel.: +81-23-647-3130; fax: +81-23-647-3109.
E-mail address: kob@ckk.ymgt-techno.or.jp (M. Kobayashi)

0168-0102/99/$ - see front matter
PII: S0168-0102(99)00040-1

Biophoton emission reflects the pathophysiological state with respect to energy (ATP) production and susceptibility to oxidative stress, which derives from excessive production of ROS or a lack of activity for antioxidant protection. Ultraweak photon emission at the subcellular level, such as isolated mitochondria (Suslova et al., 1969; Cadenas et al., 1980; Hideg et al., 1991) and at the cellular level, such as cultured carcinoma cells (Mamedov et al., 1969; Takeda et al., 1998) suggest that there is a relationship between photon emission intensity and metabolic activity.

Boveris et al. (1980) characterized photon emission from mammalian organs in an in vivo investigation of the radical reactions through lipid peroxidation. They suggested the potential usefulness for noninvasive monitoring of oxidative metabolism and oxidative damage to living tissue (Cadenas et al., 1984). Adamo et al. (1989) showed that triiodothyronine-induced hypermetabolism in a rat's brain leads to increased ultraweak photon emission as a reflection of oxidative stress and suggested that ROS contributed to premature aging in these animals.

Homogenized brain tissue also shows chemiluminescence under the condition of atmospheric auto-oxidation; and the enhancement of the intensity serves as an assay for susceptibility of lipid peroxidation resulting in peroxidate production (Imaizumi et al., 1984; Lissi et al., 1986).

We attempted to establish a technique whereby pathophysiological information can be visualized in vivo, based on highly sensitive two-dimensional photon detection technology (Amano et al., 1995; Kobayashi et al., 1996, 1997a,b). In the current paper, two-dimensional images of biophoton emission from a rat's brain detected over the skull in vivo were demonstrated for the first time; and the physiological properties of the emission associated with the metabolic activity, through simultaneous measurement of electroencephalographic (EEG) activity, are delineated. Also analyzed were the mechanisms of photon emission by using brain slices in vitro.

2. Materials and methods

2.1. Optical measurement apparatus and analysis procedures

The imaging system for biophoton emission consisted of a two-dimensional photon counting tube with a large active area, a highly efficient lens system installed in a sample chamber, and an electronic apparatus for identifying the two-dimensional spatial and temporal photoelectron data (Kobayashi et al., 1996). A block diagram is shown in Fig. 1. The photon counting tube (model IPD 440, Photek, UK) had a photocathode measuring 40 mm in diameter with spectral sensitivity (S-20) operating at a wavelength ranging from 350 to 900 nm, and with a quantum efficiency of 9% at 500, 5.5% at 600, and 1.3% at 800 nm.

The tube dark count was less than 76/s over the whole effective area with cooling at -35°C. The spatial resolution of the tube, which was determined by the readout precision of the resistive anode incorporated into the photon counting tube, was approximately 200 μm.

A specially designed lens system (Fujii Optical, Tokyo, Japan) had a 90 mm aperture with a 0.5 N.A. (numerical aperture) and 1.0 magnification, which corresponds to an image size of 25×25 mm. Output pulses from the resistive anode were fed to a position computer (IPD controller, Photek, UK) to determine the $X-Y$ position of each photoelectron event. These data (9 bits, 2 channels) were consecutively transferred to a pulse interval counter (Tohoku Electronic, Sendai, Japan) and stored with the timing data of the event, which is represented as the time interval between two successive photoelectron pulses. The time resolution of events is restricted by the position computer to a pulse-pair resolution of 10 μs.

After data acquisition, the data were transferred to a workstation (model SUN 3, Sun microsystems, CA) for reconstruction of the photon counting images and analysis of spatio–temporal properties, which demonstrated

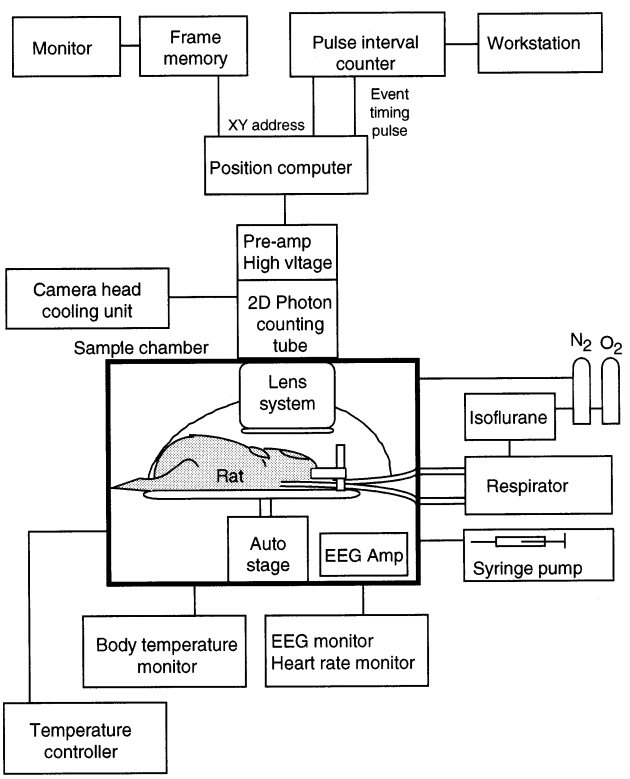

Fig. 1. A block diagram of the highly sensitive biophoton imaging system.

the intensity kinetics in the regions of interest or space–time correlation of the photoelectrons.

The images were processed as follows: (1) reduction of image format to 128×128; (2) data correction for the spatial distribution of dark counts; and (3) Gaussian smoothing over 12×12 elements. Spatial resolution after processing was approximately 2.3 mm. The minimum detectable radiant flux density, which was defined with dark counts from the detector, quantum efficiency of the photocathode, photoelectron collection efficiency, and light collection efficiency of the lens system, was experimentally evaluated and found to be 9.90×10^{-17} W/cm^2 ($= 314$ photons/s/cm^2 at a wavelength of 670 nm). A single photoelectron of the detector was estimated to correspond to 221 photons emitted onto the sample surface.

2.2. General preparation of animals

Male Wistar rats (weighing 220–300 g) were subjected to anesthesia in accordance with the NIH Guide for the Care and Use of Laboratory Animals. The animals were tracheotomized under anesthesia with pentobarbital (40 mg/kg body weight, i.p.) and artificially ventilated after cannulation of the external jugular vein for infusion (rodent respirator model 683, Harvard, MA) with a gas mixture of 1% isoflurane in 45% oxygen and 55% nitrogen. The rats were immobilized by pancuronium bromide (1 mg/kg, i.v) and an additional dose (1 mg/kg/h) was subsequently infused with 1 ml/h saline, using a syringe pump (model TOP-5200, TOP, Tokyo, Japan).

The rats were surgically prepared with an incision of the skin to expose the skull. To remove the skull, the parietal bones were removed bilaterally, leaving the dura mater. The area to be observed was covered with a transparent film to prevent the surface from drying. The areas surrounding the target were covered with a thick black cloth. To reduce the effect of phosphorescence caused by lighting during surgical preparation, we avoided exposure to fluorescent light. To record EEG activity, silver ball electrodes were inserted into the skull over both hemispheres. The rectal temperature was monitored throughout the experiment and maintained at 38.2 ± 0.5°C by a hot water blanket.

Forebrain ischemia was produced by using a four-vessel occlusion model (Yoshida et al., 1982). On the day before the scheduled experiment, the vertebral arteries were occluded bilaterally, followed by bilateral (but reversible) ligation of the common carotid artery.

2.3. Sample setting and measurement

Each rat was mounted on a stereotaxic frame and placed under the lens system in a completely light-tight chamber. After focusing with weak light illumination and dark adaptation to reduce phosphorescence (1 h), measurement was started. The period for dark adaptation was decided from the actual measurements, in which we found that the initial intensities of phosphorescence were not exceeded by twice the steady level of intensity and the time constants were ranged within approximately 30–60 min. Consequently, phosphorescence in most cases was negligible after 1 h.

Atmospheric gas in the chamber was replaced with nitrogen ($> 99\%$) to prevent artificial chemiluminescence induced by auto-oxidation of the exposed tissue surface. The EEG was recorded through differential amplifiers with a voltage gain of 10^4, and recorded at a sampling rate of 100 sampling points/s. The θ-wave component (4–7 Hz) of the power spectral density of the EEG was extracted to evaluate brain activity.

2.4. Experiments with brain slices

The techniques for preparing and maintaining brain slices were almost identical to those described previously (Fujii et al., 1991). After decapitation under diethyl ether anesthesia, frontally sectioned 500 μm thick slices of a hemisphere were prepared by using a Rotoslicer (model DTY-7700, Dosaka EM, Kyoto, Japan). Approximately 10 sheets of slices were placed in a quartz chamber, which measured 46 mm in diameter and 5 mm in depth, with a circulating artificial cerebrospinal fluid (ACSF) bubbled with 95% O_2 and 5% CO_2 at a flow rate of 2 ml/min. Photon emission intensity was measured, using a photon counting system (Kobayashi et al., 1998), which was incorporated into a photomultiplier tube (model R1333, Hamamatsu Photonics, Hamamatsu, Japan).

The temperature of ACSF was monitored continuously and carefully controlled at 30 ± 0.1°C. The sample chamber was filled with a gas mixture of 95% N_2 and 5% CO_2.

3. Results

3.1. Ultraweak photon emission images of normal rat brain

In Fig. 2a, a typical example of an ultraweak biopho-

Fig. 2. (a) Ultraweak photon emission image of a normal rat's brain observed outside the skull, compared with (b) an image during brain ischemia, consecutively obtained by (a). Integration time is 1 h in both cases. Image size is 25×25 mm. (c) Three-dimensional display of (a). (d) Three-dimensional display of (b). (e) Sample image obtained under weak light illumination. (f) Schematic illustration of the observation field. Fig. 4. (a) Image of ultraweak photon emission from a rat's brain with the insertion of a thin plate under the skull for light shielding. (b) The image obtained after removing the plate. Integration time is 1 h. (c) Schematic illustration indicating the region that is shielded by the plate.

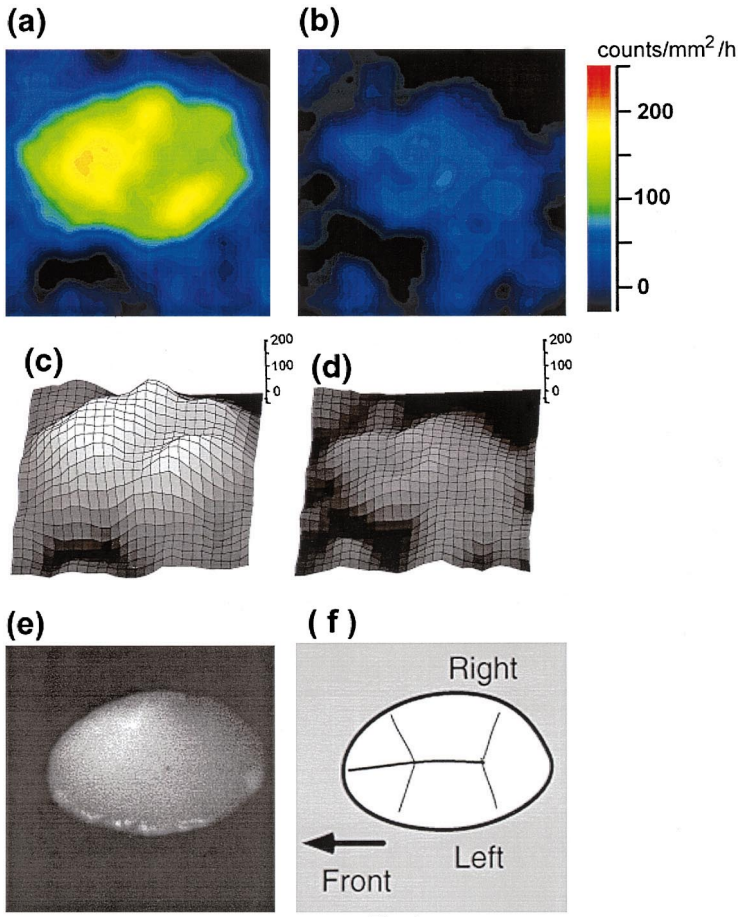
(a)
(b)
counts/mm2/h
200
100
0
(c)
(d)
200
100
0
(e)
(f)
Right
Left
Front

Fig. 2

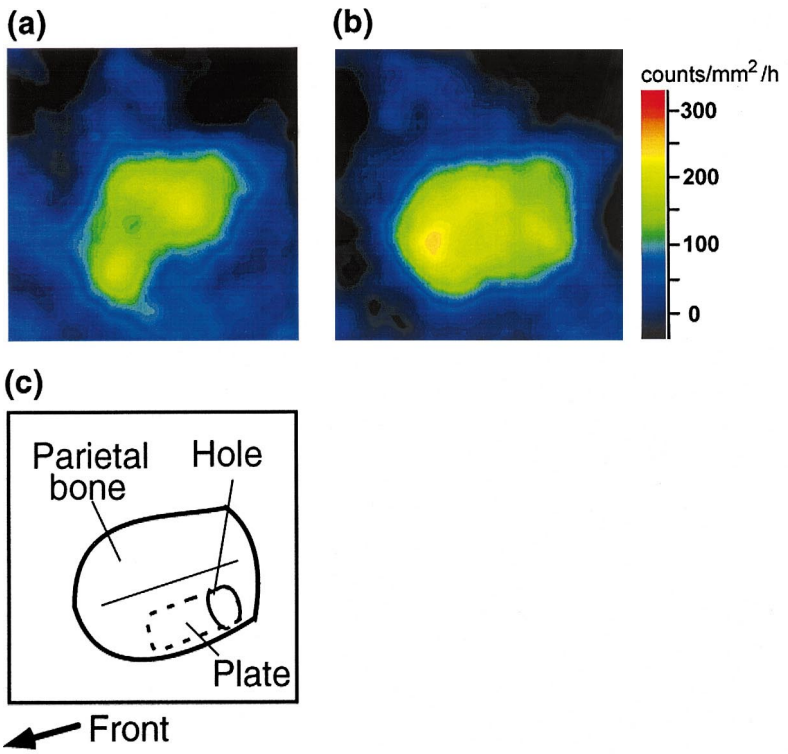
(a)
(b)
counts/mm2/h
300
200
100
0
(c)
Parietal bone
Hole
Plate
Front

Fig. 4

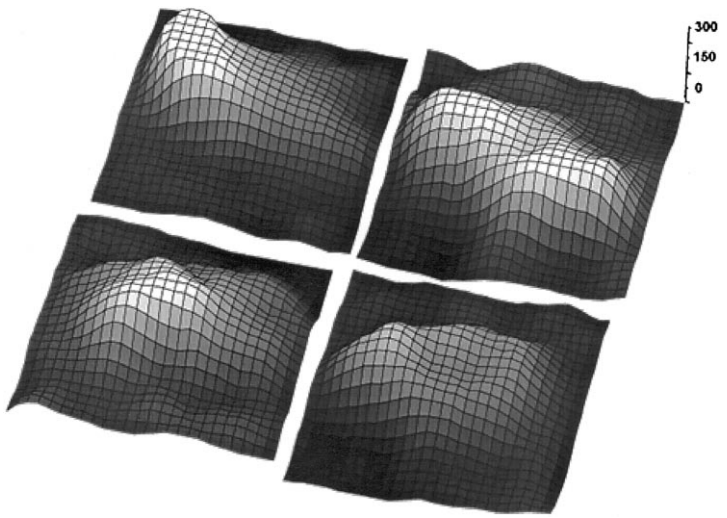

Fig. 3. Comparison of ultraweak photon emission images of four individual normal rats' brain observed outside the skull under the same conditions.

ton emission image of a normal rat brain observed over the skull is illustrated. The image obtained from the same animal for the consecutive measurement during brain ischemia with a flat EEG is shown in Fig. 2b. Fig. 2c and d are three-dimensional expression of images from Fig. 2a and b, respectively, for quantitative evaluation of the images.

The integration time for both images was 1 h, and the average counts on the brain region changed from 138 to 27.9 counts/mm^2/h with subtraction of background intensity. The intensity during ischemia was comparable to that after cardiac arrest. As the shot noise level of the images determined in the current condition of space and time resolution was estimated to 9.73 counts/mm^2/h, the intensity distribution shown in the image was regarded to be significantly different. The comparison of images obtained from four individual animals under the normal condition is indicated in Fig. 3, designating the common tendency of intensity distribution, as the frontal region is relatively brighter than the back region.

To clarify the origin of the photon emission, a thin plate was inserted to shield light from the cortex. An opaque plate made of synthetic resin (0.5 mm thick) was carefully inserted into a drilled hole in the skull, between the dura mater and parietal bone (Fig. 4c). The region lacking intensity (38.0 counts/mm^2/h) corresponded to the inserted site (Fig. 4a) with the intensity reduced to approximately 1/3 in comparison with the image taken after removing the plate (128.0 counts/mm^2/h) (Fig. 4b). This suggested that photons emanating from the brain tissue and going through the skull are the chief contributors to the biophoton image.

3.2. Correlation between photon emission intensity and EEG activity

An example of the time course of biophoton emission intensity and simultaneously measured EEG activity represented by the θ-wave component of the EEG power spectrum is displayed in Fig. 5a. Temporal changes of the photon emission intensity were relatively comparable to the θ-wave activity. Changes in the spatial pattern of emission were also observed from images in the respective time regions, as shown in Fig. 5b.

Fig. 6a and b show the results of correlation analysis between photon emission intensity and θ-wave activity, represented by 30-min integration under a different condition of skull treatment. Fig. 6a shows the result obtained from four animals where the parietal bones were removed, and Fig. 6b that obtained over the skull from 11 animals. Both figures have been composed by superimposing independent measurements. Although emission intensities observed through the skull are approximately one-half of those with the parietal bones removed, both results support the correlation between photon emission intensity and the θ-wave component of the EEG power spectra, with statistical significance ($P < 0.001$).

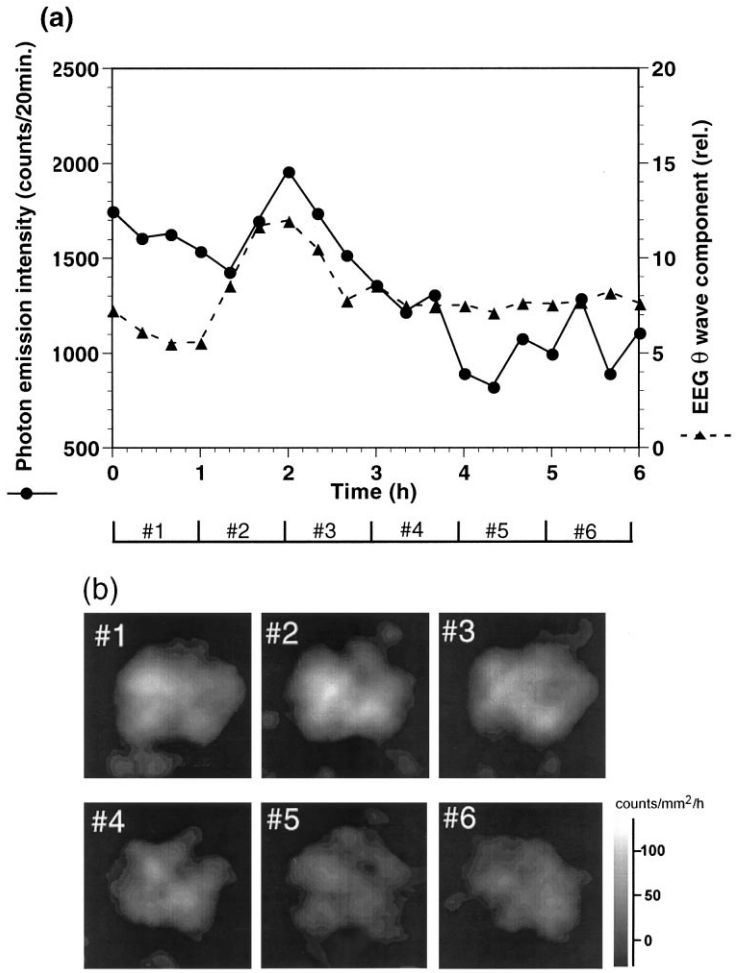

Fig. 5. (a) An example of temporal changes in ultraweak photon emission intensity from a rat's brain and the θ-wave component of EEG power spectral density (ratio of component expressed in percent, relative). (b) Sequential images of photon emission for the time regions of #1–#6, indicated in (a).

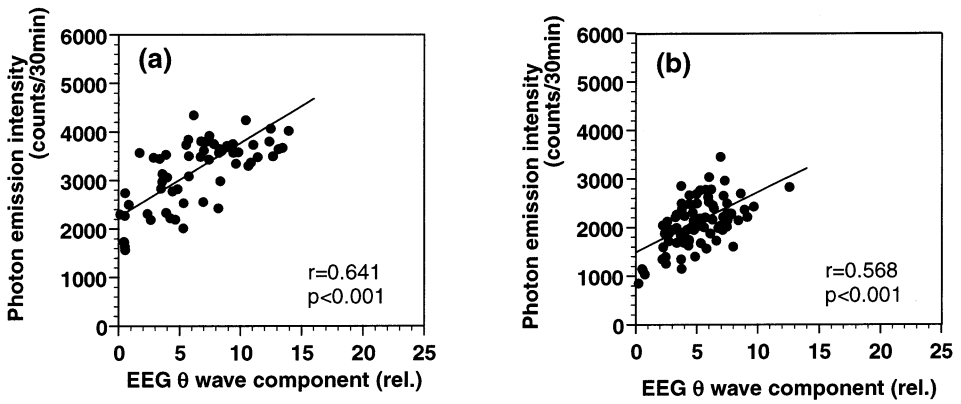

Fig. 6. Correlation analysis between photon emission intensity and the θ-wave component of EEG power spectra represented by 30-min integration. (a) Correlation after having the bilateral bones removed and (b) without removing the bone. The correlation coefficients and statistical significance are indicated in the figures.

3.3. Ultraweak photon emission images under hyperoxia-induced oxidative stress

Fig. 7 shows intensity changes in photon emission under varying concentrations of inhaled oxygen. Photon emission intensity measured during hyperoxia (inhaled O_2, 100%) was enhanced to approximately 130% in comparison with the normal condition (inhaled O_2, 45%). With the oxygen concentration restored to 45%, the photon emission intensity decreased gradually instead of a quick reduction. The image of photon emission for each stage is shown in Fig. 7b.

Under the normal condition before hyperoxia (Fig. 7b, # 1), the photon emission intensity was relatively high in the frontal region (average intensity of the frontal region was 127% of the dorsal region). During hyperoxia (Fig. 7b, # 2), the emission intensity increased in the whole area, with weight on the frontal region. Having returned to the normal oxygen concentration (Fig. 7b, # 3), the photon emission intensity at the frontal region was enhanced in comparison with that before hyperoxia; and 1 h later a bright area was observed on the right-frontal region (Fig. 7b, # 4). For three individual experiments under the same conditions a characteristic pattern for the localization of photon emission was observed only in this case. Although the cause of the localization was not clear, these characteristic patterns of spatial distribution were examined as potential indices for the localization of ROS generation, depending on the regional susceptibility to oxidation.

3.4. Ultraweak photon emission from brain slices

To investigate the mechanism of photon emission, in vitro experiments were continued by using brain slices and varying the parameters related to energy metabolism and cellular respiration. Photon emission intensity from the slices depended strictly on temperature and oxygen concentrations of ACSF. Under an ACSF temperature of 30°C, the time course of emission intensity decreased in the first 15 min, then it slightly increased to reach a steady level within 1 h.

The initial decrease of photon emission may be due to the phosphorescence of the slices; and the subsequent increase may be the result of propagation of auto-oxidation. The changes in photon emission caused by chemicals were observed approximately 1.5 h after sample setting. Fig. 8 shows typical examples of the time courses of emission intensity changes caused by various agents. When glucose was removed from the ACSF (Fig. 8a), the photon emission intensity was suppressed to $79.0 \pm 4.5\%$ (mean $\pm$ S.E.M., $n = 4$) of the control 1

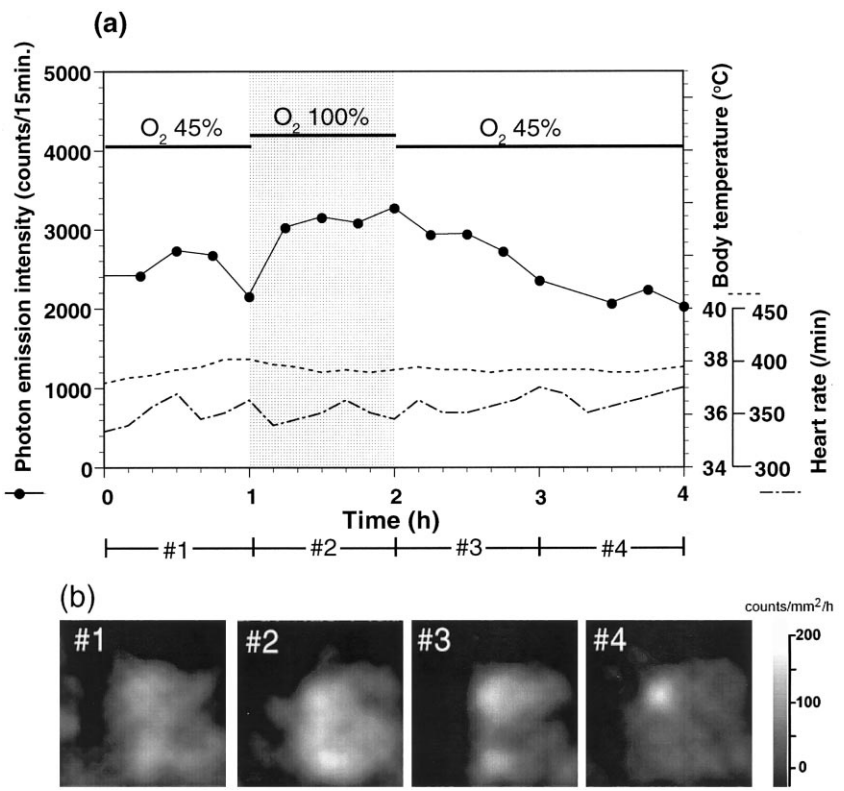

Fig. 7. (a) An example of the time course of ultraweak photon emission intensity before, during, and after hyperoxia (—) with simultaneously measured body temperature (···) and heart rate (–·–·). (b) Ultraweak photon emission images of the brain in time regions of # 1– # 4, indicated in (a).

h after the removal. The addition of 50 mM KCl to ACSF led to a transient increase of photon emission within a few minutes after drug administration but the condition subsequently depressed the intensity to $89.5 \pm 4.3\%$ ($n = 3$) (Fig. 8b) of the control.

Fig. 8c shows the increase in photon emission induced by the addition of 10 mM glutamate. The intensity of photon emission gradually increased and remained at a steady level for more than 1 h after the glutamate was washed out. It reached $124.4 \pm 5.7\%$ ($n = 4$) 30 min after administration. Acute intensity changes corresponding to neuronal activation even by addition of 1 mM glutamate were observed to be absent except for a gradual increase of photon emission.

We examined the effects of rotenone (20 μM) and antimycin-A (20 μM), inhibitors of respiration by the mitochondrial electron transport chain. A continuous increase of photon emission was observed in both instances. Fig. 8d shows the time courses of emission when the preparations were treated with 20 μM rotenone. The intensity of the photon emission temporally decreased to approximately 90% of the level before administration.

After 15 min the increase continued, reaching $124.0 \pm 5.8\%$ ($n = 3$) 1 h after administration. Rotenone administration under glucose deprivation brought the intensity to early saturation (Fig. 8d, dotted line). When antimycin-A was applied the photon emission intensity increased, generally simulating the pattern observed when rotenone was administered (data not shown).

4. Discussion

In general brain tissue accounts for approximately 20% of the whole body oxygen consumption and contains a comparatively high concentration of polyunsaturated fatty acids. It is known to be very susceptible to radical injuries subsequent to ROS generation. Oxidative stress, for example under postischemic reperfusion, leads to lipid peroxidation and oxidative injury (Traystman et al., 1991), focally affecting selectively vulnerable regions of the brain (Watson et al., 1984; Bromont et al., 1988; Globus et al., 1995). Therefore, in situ identification of the spatio–temporal properties of oxidative stress is most valuable and important for the investigation of radical injuries.

Although ultraweak photon emission phenomena in normal mammalian organs associated with lipid peroxidation or other radical reactions are generally known, the spatial distribution of biophoton emissions has not been clarified because they are weak. The present study demonstrated in vivo imaging of ultraweak photon emissions from a normal rat's brain, using a highly sensitive photon counting imaging system equipped with a large sensitive area. The photon emission intensity was characterized by and found to correlate with cerebral blood flow and EEG activity, while hyperoxia induced an enhancement of the intensity with the spatial localization of photon emission.

Based on the experimental results of plate insertion (Fig. 4), correlation with EEG activity, and the comparison with different conditions of skull treatment

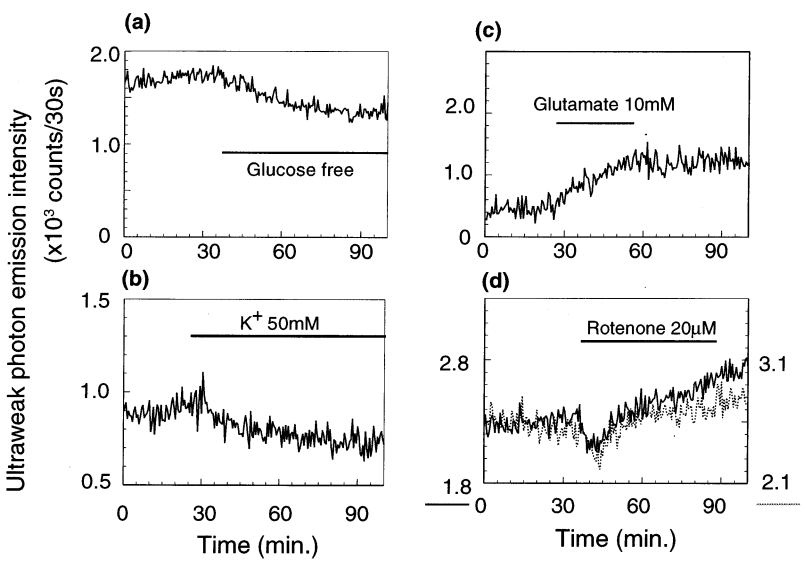

Fig. 8. Temporal changes in ultraweak photon emission intensity from brain slices under various conditions. (a) Glucose deprivation, (b) addition of 50 mM KCl, (c) addition of 10 mM glutamate, and (d) effect of 20 μM rotenone under the condition of 10 mM glucose (—) in standard ACSF and glucose free (···).

(Fig. 6), it has been deduced that ultraweak photon emission observed from outside the skull originates mainly from the cortex. With consideration given to the optical penetration depth of the brain tissues, which is reported to be approximately 0.5–1.0 mm in visible wavelength (Eggert and Blazek, 1987), the origin of emission may be superficial, consisting mostly of gray matter in the cortex. Highly sensitive two-dimensional photon detection techniques may reveal the pathophysiological information on the cortex by imaging of biophotons from outside the skull.

In vitro experiments suggest that intracellular respiration of mitochondria for energy (ATP)-yielding metabolism participates in photon emission. The suppression of photon emission intensity under glucose deprivation implies that approximately 20% of the emission is associated with cellular respiration. The condition remains independent of the substrate involved in energy metabolism and may be derived by auto-oxidation of samples under high concentrations of oxygen.

It is known that a high concentration of potassium ions increases oxygen uptake: this is referred to as the potassium effect. The temporal enhancement of photon emission induced by 50 mM of potassium ions (Fig. 8b) may represent the increased cellular respiration. By using hippocampal slices, Isojima et al. (1995) also reported an increase in ultraweak photon emission that corresponded to the potassium effect. This can be explained as an increase in energy metabolism due to $Na^+ + K^+$-ATPase activation (Gubitz et al., 1977). The subsequent decrease in intensity after the temporal enhancement implies a reduction in energy metabolism as the result of cellular dysfunction.

Glutamate (10 mM) also causes the photon emission intensity to increase. However, the time course of a continuous increase in photon emission does not approximate the pattern associated with 50 mM K^+. Because excitatory amino acids are known to facilitate oxygen consumption and a high concentration of glutamate (10 mM), in particular, increases the oxygen uptake through glutamate metabolism as the substrate for oxidative phosphorylation (Nishizaki and Okada, 1988), the enhancement of photon emissions might be related to glutamate metabolism. Although the photon emission response induced by neuronal stimulation was not detected, the delayed increase of photon emissions appears to be caused by glutamate metabolism, or might be the reflection of oxidative stress induced by excessive activation of the glutamate receptors (Coyle and Puttfarcken, 1993).

The respiratory chain of inner mitochondrial membranes usually leads to ROS production through univalent and bivalent reduction of oxygen. The process is accelerated especially in highly reduced states. Intracellular levels of ROS are governed by antioxidant species under general control of the enzymatic or nonenzymatic protection system. For example in a rat's liver, intracellular steady-state levels of these radicals have been reported to be about 10^{-11}–10^{-10} M for $O_2^{-\bullet}$ and 10^{-8}–10^{-7} M for H_2O_2 (Chance et al., 1979). In brain mitochondria, the H_2O_2 level is estimated to be approximately 10^{-8} M without considering glutathione peroxidase activity (Adamo et al., 1989).

The effects of respiration inhibitors on the intensity of photon emission in our experiments support the involvement of the mitochondrial electron transport chain for photon emission and the contribution of ROS production through the cellular respiratory process. The initial decrease in photon emission observed after administration of rotenone (Fig. 8d) may correspond to the suppression of energy metabolism; and the subsequent increase in intensity should be the result of continuous generation of ROS and a decline in the capacity of scavengers. The difference in time course between 'with and without glucose' also supports the notion that the origin of the rotenone-induced photon emission is derived from the mitochondrial electron transport chain. Rotenone blocks the reduction of ubiquinone by NADH dehydrogenase and antimycin-A inhibits ubiquinone-cytochrome C reductase. Thus a possible leakage site in the electron transport chain for the direct reduction of O_2 seems to be in compounds I and II (Cino and Maestro, 1989).

It is suspected that excited species for photon emission are formed through a radical reaction with ROS and intracellular substances. Particularly in the case of unsaturated fatty acids, excited species are generated as the result of a lipid peroxidation process initiated by H_2O_2, metal-catalyzed $OH^{\bullet}$, or enzymatically produced ROS (Cadenas et al., 1984). The origin of emission species might be the excited carbonyl and singlet oxygen derived through the Russel mechanism (Cadenas et al., 1984; Murphy and Sies, 1990), as a terminal reaction to the lipid peroxidation process. Excited protein that consists of enzymatically generated excited tyrosine or tryptophan (Nakano, 1989) is also suspected. Ultraweak biophoton emission in vivo is deduced as a result of oxidative side reactions underlying energy metabolism through inner mitochondrial ROS generation (Adamo et al., 1989). The correlation between photon emission intensity and EEG activity in vivo is interpreted as the participation of massive and basal energy metabolism in the cortex under normal physiological conditions. However, considering the in vitro results of administering glutamate, activation of neuronal metabolism directly accompanying electrophysiological activity seems to be less effective for biophoton emission.

Augmenting photon emission to approximately 150% by hyperoxia (Fig. 7) suggests the reflection of oxidative stress. It was reported that hyperoxia augments the in vivo production of H_2O_2 in a rat's brain linearly to 160% of air inhalation (Yusa et al., 1987), which is interpreted

as overproduction of ROS and a loss of efficiency in the scavenging system (Yusa et al., 1987). The temporal increase in the first 30 min of hyperoxia may represent the progression of oxidative stress, which is presumed to be a gradual inactivation of the antioxidant system. A gradual decrease after returning to the normal concentration of O_2 can be explained as an indication of the recovery process from oxidative stress.

Enhanced chemiluminescence methods have recently come to be applied commonly for ROS detection. Dirnagl et al. (1995) reported that superoxide production is induced by oxidative stress under hyperoxia or postischemic reperfusion, based on lucigenin-enhanced chemiluminescence, by using an in situ preparation (without imaging).

Although biophoton emissions without an enhancer are extremely weak due to the low efficiency of the excitation mechanism, the measurement of spontaneous photon emission has the advantage of being a native reflection of physiological and pathological conditions. Therefore two-dimensional imaging of ultraweak photon emissions has the potential to delineate the spatial distribution of energy metabolism and to visualize the oxidative stress and damage to the cortex: it is believed that the characteristic kinetics of emission intensity illustrates a pathophysiological response of the central nervous system.

References

Adamo, A.M., Llesuy, S.F., Pasquini, J.M., Boveris, A., 1989. Brain chemiluminescence and oxidative stress in hyperthyroid rats. Biochem. J. 263, 273–277.

Amano, T., Kobayashi, M., Devaraj, B., Usa, M., Inaba, H., 1995. Ultraweak biophoton emission imaging of transplanted bladder cancer. Urol. Res. 23, 315–318.

Boveris, A., Cadenas, E., Reiter, R., Filipkowski, M., Nakase, Y., Chance, B., 1980. Organ chemiluminescence: noninvasive assay for oxidative radical reactions. Proc. Natl. Acad. Sci. USA 77, 347–351.

Bromont, C., Marie, C., Bralet, J., 1988. Increased lipid peroxidation in vulnerable brain regions after transient forebrain ischemia in rats. Stroke 20, 918–924.

Cadenas, E., Boveris, A., Chnace, B., 1980. Low-level chemiluminescence of bovine heart submitochondrial particles. Biochem. J. 186, 659–667.

Cadenas, E., Boveris, A., Chance, B., 1984. Low-level chemiluminescence of biological systems. In: Proyor, W.A. (Ed.), Free Radicals in Biology, vol. 4. Academic Press, New York, pp. 211–242.

Chance, B., Sies, H., Boveris, A., 1979. Hydroperoxide metabolism in mammalian organs. Physiol. Rev. 59, 527–605.

Cilent, G., 1988. Photobiochemistry without light. Experientia 44, 572–575.

Cino, M., Maestro, F.D., 1989. Generation of hydrogen peroxide by brain mitochondria: the effect of reoxygenation following postdecapitative ischemia. Arch. Biochem. Biophys. 269, 623–638.

Coyle, J.T., Puttfarcken, P., 1993. Oxidative stress, glutamate, and neurodegenerative disorders. Science 262, 689–695.

Devaraj, B., Usa, M., Inaba, H., 1997. Biophotons: ultraweak light emission from living systems. Curr. Opin. Solid State Mat. Sci. 2, 188–193.

Dirnagl, U., Lindauer, U., Them, A., et al., 1995. Global cerebral ischemia in the rat: online monitoring of oxygen free radical production using chemiluminescence in vivo. J. Cereb. Blood Flow Metab. 15, 929–940.

Eggert, H.R., Blazek, V., 1987. Optical properties of human brain tissue, menings, and brain tumors in spectral range of 200 to 900 nm. Neurosurgery 21, 459–464.

Fujii, S., Saito, K., Miyakawa, H., Ito, K.-I., Kato, H., 1991. Reversal of long-term potentiation (depotentiation) induced by tetanus stimulation of the input to CA1 neurons of guinea pig hippocampal slices. Brain Res. 555, 112–122.

Globus, M.Y.-T., Busto, R., Lin, B., Schnippering, H., Ginsberg, M.D., 1995. Detection of free radical activity during transient global ischemia and recircuration: effects of intraischemic brain temperature modulation. J. Neurochem. 65, 1250–1256.

Gubitz, R.H., Akera, T., Brody, T.M., 1977. Control of brain slice respiration by $(Na^+ + K^+)$-activated adonosine triphosphatase and the effects of enzyme inhibitors. Biochim. Biophys. Acta 459, 263–277.

Hideg, E., Kobayashi, M., Inaba, H., 1991. Spontaneous ultraweak light emission from respiring spinach leaf mitochondria. Biochim. Biophys. Acta 1098, 27–31.

Imaizumi, S., Kayama, T., Suzuki, J., 1984. Chemiluminescence in hypoxic brain—the first report; correlation between energy metabolism and free radical reaction. Stroke 15, 1061–1065.

Inaba, H., 1988. Super-high sensitivity systems for detection and spectral analysis of ultraweak photon emission from biological cells and tissues. Experientia 44, 550–559.

Isojima, Y., Isoshima, T., Nagai, K., Kikuchi, K., Nakagawa, H., 1995. Ultraweak biochemiluminescence detected from rat hippocampal slices. NeuroReport 6, 658–660.

Kobayashi, M., Devaraj, B., Usa, M., Tanno, Y., Takeda, M., Inaba, H., 1996. Development and applications of new technology for two-dimensional space–time characterization and correlation analysis of ultraweak biophoton information. Frontiers Med. Biol. Eng. 7, 299–309.

Kobayashi, M., Devaraj, B., Usa, M., Tanno, Y., Takeda, M., Inaba, H., 1997a. Two-dimensional imaging of ultraweak photon emission from germinating soybean seedlings with a highly sensitive CCD camera. Photochem. Photobiol. 65, 535–537.

Kobayashi, M., Takeda, M., Yoshida, M., et al., 1997b. The first demonstration of 2D-imaging of ultraweak biophoton emission from rat brain in vivo. Med. Biol. Eng. Comput. 35 Suppl., 673.

Kobayashi, M., Devaraj, B., Inaba, H., 1998. Observation of super-Poisson statistics of bacterial (*Photobacterium phosphoreum*) bioluminescence during the early stage of cell proliferation. Phys. Rev. E 57, 2129–2133.

Lissi, E.A., Caceres, T., Videla, L.A., 1986. Visible chemiluminescence from rat brain homogenates undergoing autoxidation. I. Effect of additives and products accumulation. Free Radic. Biol. Med. 2, 63–69.

Mamedov, T.G., Podov, G.A., Konev, V.V., 1969. Ultraweak luminescence of various organisms. Biofizika 14, 1047–1051.

Murphy, M.E, Sies, H., 1990. Visible-range low-level chemiluminescence in biological systems. Methods Enzymol. 186, 595–610.

Nakano, M., 1989. Low-level chemiluminescence during lipid peroxidations and enzymatic reactions. J. Biolum. Chemilum. 4, 231–240.

Nishizaki, T., Okada, Y., 1988. Effects of excitatory amino acids on the oxygen consumption of hippocampal slices from the guinea pig. Brain Res. 452, 11–20.

Popp, F.-A., 1988. Biophoton emission. Experientia 44, 543–544.

Popp, F.-A., Li, K.H., Mei, W.P., Galle, M., Neurohr, R., 1988. Physical aspects of biophotons. Experientia 44, 576–585.

Slawinski, J., 1988. Luminescence research and its reaction to ultraweak cell radiation. Experientia 44, 559–571.

Suslova, T.B., Olenev, V.I., Vladimirov, Y.A., 1969. Chemiluminescence coupled with the formation of lipid peroxides in biological

membranes—I. Luminescence of mitochondria on addition of Fe^{++}. Biofizika 14, 540–548.

Takeda, M., Tanno, Y., Kobayashi, M., Usa, M., Inaba, H., 1998. A novel method of assessing carcinoma cell proliferation by biophoton emission. Cancer Lett. 127, 155–160.

Traystman, R.J., Kirsch, J.R., Koehler, R.C., 1991. Oxygen radical mechanisms of brain injury following ischemia and reperfusion. J. Appl. Physiol. 71, 1185–1195.

Usa, M., Devaraj, B., Kobayashi, M., et al., 1994. Detection and characterization of ultraweak biophotons from life processes. In: Ohzu, H., Komatsu, S. (Eds.), Optical Methods in Biomedical and Environmental Sciences. Elsevier, Amsterdam, pp. 3–6.

Van Wijk, R., Schamhart, D.H.J., 1988. Regulatory aspects of low intensity photon emission. Experientia 44, 586–593.

Watson, B.D., Busto, R., Goldberg, W.J., Santiso, M., Yoshida, S., Ginsberg, M.D., 1984. Lipid peroxidation in vivo induced by reversible global ischemia in rat brain. J. Neurochem. 42, 268–274.

Yoshida, S., Abe, K., Busto, R., Watson, B.D., Kogure, K., Ginsberg, M.D., 1982. Influence of transient ischemia on lipid-soluble antioxidants, free fatty acids and energy metabolites in rat brain. Brain Res. 245, 307–316.

Yusa, T., Beckman, J.S., Crapo, J.D., Freeman, B.A., 1987. Hyperoxia increases H_2O_2 production by brain in vivo. J. Appl. Physiol. 63, 353–358.